



## Modelling probabilistic fatigue crack propagation rates for a mild structural steel

J.A.F.O. Correia, A.M.P. de Jesus  
*University of Trás-os-Montes e Alto Douro, Vila Real, Portugal*  
*UCVE-IDMEC-LAETA, Porto, Portugal*  
*jcorreia@utad.pt, ajesus@utad.pt*

A. Fernández-Canteli  
*University of Oviedo*  
*afc@uniovi.es*

R.A.B. Calçada  
*Faculty of Engineering, University of Porto, Porto, Portugal*  
*ruiabc@fe.up.pt*

---

**ABSTRACT.** A class of fatigue crack growth models based on elastic–plastic stress–strain histories at the crack tip region and local strain-life damage models have been proposed in literature. The fatigue crack growth is regarded as a process of continuous crack initializations over successive elementary material blocks, which may be governed by smooth strain-life damage data. Some approaches account for the residual stresses developing at the crack tip in the actual crack driving force assessment, allowing mean stresses and loading sequential effects to be modelled. An extension of the fatigue crack propagation model originally proposed by Noroozi *et al.* (2005) to derive probabilistic fatigue crack propagation data is proposed, in particular concerning the derivation of probabilistic  $da/dN$ - $\Delta K$ - $R$  fields. The elastic-plastic stresses at the vicinity of the crack tip, computed using simplified formulae, are compared with the stresses computed using an elastic-plastic finite element analyses for specimens considered in the experimental program proposed to derive the fatigue crack propagation data. Using probabilistic strain-life data available for the S355 structural mild steel, probabilistic crack propagation fields are generated, for several stress ratios, and compared with experimental fatigue crack propagation data. A satisfactory agreement between the predicted probabilistic fields and experimental data is observed.

**KEYWORDS.** Fatigue, Crack propagation, Fracture mechanics, Local approach, Probabilistic approach, Finite Element Modelling.

---

### INTRODUCTION

Fatigue of materials and structures has been investigated for more than 150 years [2]. Although it still attracts a lot of attention of engineers and scientists. Concerning the investigation of the fatigue crack propagation, significant developments were carried out since the original Paris *et al.* [3] milestone contribution. Paris *et al.* [3] was pioneer suggesting the stress intensity factor range as a crack driving force parameter. The so-called Paris's law stated this relation

---



in a very simple form: the power function. It has been rather documented in the literature the Paris's law limitations [4]: i) it only models stable fatigue crack propagation behaviour (propagation regime II) and ii) does not account for stress ratio effects. Many alternative fatigue crack propagation relations have been proposed to overcome the limitations of the Paris's law and also to deal with variable amplitude loading. Nevertheless, the Paris's law still has been intensively used to model fatigue crack growth under constant amplitude loading due to its attractive simplicity. The number of parameters involved in the more comprehensive fatigue crack propagation models may increase significantly which makes their evaluation a costly task and very often discouraging engineers of their application.

Fatigue crack growth testing is costly and alternative less expensive approaches to derive fatigue crack growth data are consequently welcome. Local strain-based approaches [5-8] were originally proposed to model fatigue crack initiation on notched components [9]. A link between the local strain-based approaches to fatigue and the Fracture Mechanics based fatigue crack propagation models has been proposed by some authors [1, 10-14]. Glinka [13] was one of the first researchers to use the local strain approaches to model fatigue crack propagation. The original idea of Glinka was later followed and developed by his collaborators, such as Noroozi *et al.* [1, 10-11], using crack tip residual stress concepts to explain stress ratio effects as well as loading interaction effects on fatigue crack growth rates. Pecker and Niemi [12], based on the original idea of Glinka, made also independent contributions, using crack closure concepts to explain stress R-ratio and load interaction effects. In general, elastoplastic stress analysis at the crack tip vicinity has been performed using analytical approaches, however numerical approaches based on finite element analysis were followed by Hurley and Evans [14].

The underlying concept behind the proposed local approaches for fatigue crack propagation modelling consists of assuming fatigue crack propagation as a process of continuous failure of consecutive representative material elements (continuous re-initializations). Such a kind of approaches has been demonstrated to correlate fatigue crack propagation data from several sources, including the stress ratio effects [1, 10-14]. The crack tip stress-strain fields are computed using elastoplastic analysis, which are applied together a fatigue damage law to predict the failure of the representative material elements. The simplified method of Neuber [15] or Moftakhar *et al.* [16] may be used to compute the elastoplastic stress field at the crack tip vicinity using the elastic stress distribution given by the Fracture Mechanics [1, 16-17].

This paper proposes an assessment and extension of the model proposed by Noroozi *et al.* [1, 10-11] to predict the fatigue crack propagation rates, based on local strain approach to fatigue. This model has been denoted as UniGrow model and classified as a residual stress based crack propagation model [18]. The model is applied in this paper to derive probabilistic fatigue crack propagation  $da/dN$ - $\Delta K$  fields for the S355 structural mild steel, for distinct stress R-ratios ( $p$ - $da/dN$ - $\Delta K$ -R). Results are compared with available experimental fatigue crack propagation data from testing of compact tension specimens [19]. A central parameter in the UniGrow model is the material representative element size,  $\rho^*$ , which is tuned in this research by means of a trial and error procedure. The elastoplastic stresses at the vicinity of the crack tip are computed using both simplified formulae and elastoplastic finite element analyses for comparison purposes. The deterministic strain-life damage relation adopted in the original UniGrow model is replaced by a probabilistic counterpart. The probabilistic model as proposed by Castillo and Fernández-Canteli [20] for the strain-life field, based on Weibull distribution, was generalized in order to incorporate a damage parameter definition able to account for mean stress effects. In particular, the Smith-Watson-Topper damage parameter was selected resulting the  $p$ - $SWT$ - $N$  which was applied to derive the probabilistic crack propagation fields.

## THEORETICAL BACKGROUND

In this section, an overview of the UniGrow model that has been proposed to predict the fatigue crack growth by means of a local approach to fatigue, is presented. Also, a recently proposed probabilistic strain-life model is introduced. An extension/generalization of the probabilistic strain-life approach, to account for mean stress effects, is proposed which will be applied latter, in this chapter, in conjunction with the UniGrow model to predict probabilistic fatigue crack propagation data.

### *Overview of the deterministic UniGrow model*

The UniGrow model as proposed by Noroozi *et al.* [1] is supported on the following assumptions:

- The material is composed of elementary particles of a finite dimension  $\rho^*$  also called material representative elements, below which material cannot be regarded as a continuum, Fig. 1.a);
- The fatigue crack tip is considered equivalent to a notch with a radius equal to  $\rho^*$ , Fig. 1.b).

- The fatigue crack growth results from a process of successive crack increments due to crack re-initializations over the distance  $\rho^*$ . Thus, the fatigue crack growth rate can be established according the following relation:

$$\frac{da}{dN} = \frac{\rho^*}{N_f} \quad (1)$$

where  $N_f$  is the number of cycles required to fail the material representative element, which can be computed using a fatigue damage relation such as the so-called strain-life relations.

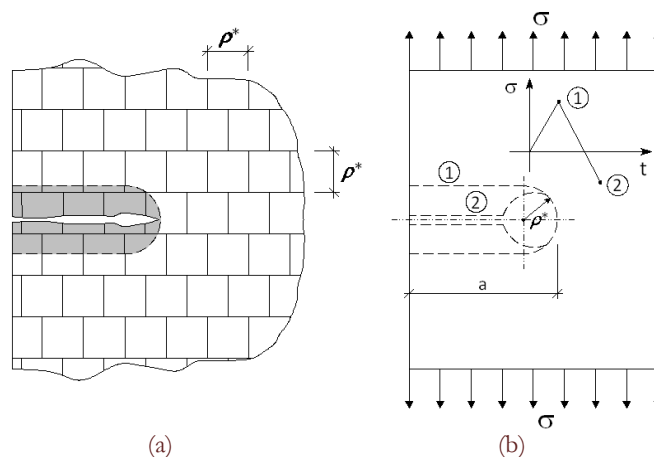


Figure 1: Crack configuration according to the UniGrow model: a) crack and the discrete elementary material blocks; b) crack geometry at the tensile maximum and compressive minimum loads [1].

Noroozi *et al.* [1] suggested the use of a strain-life relation based on Smith, Watson and Topper fatigue damage parameter [8]:

$$\sigma_{\max} \cdot \Delta\varepsilon/2 = SWT = (\sigma'_f)^2 \cdot (2N_f)^{2b} / E + \sigma'_f \cdot \varepsilon'_f \cdot (2N_f)^{b+c} \quad (2)$$

Alternatively, Peeker and Niemi [12] in a similar approach for the fatigue crack propagation suggested the use of the Morrow's equation [7] to compute the failure of the material representative element:

$$\frac{\Delta\varepsilon}{2} = \frac{\sigma'_f - \sigma_m}{E} \cdot (2N_f)^b + \varepsilon'_f \cdot (2N_f)^c \quad (3)$$

The Morrow's equation was derived from the Coffin-Manson relation [6, 7] of the material, and allows mean stress effects to be accounted for:

$$\frac{\Delta\varepsilon}{2} = \frac{\sigma'_f}{E} \cdot (2N_f)^b + \varepsilon'_f \cdot (2N_f)^c \quad (4)$$

SWT-life equation, Eq. (2), was originally derived by the multiplication of the Coffin-Manson Eq. (4) by the Basquin relation [21] available for a stress R-ratio equal to  $-1$ :

$$\frac{\Delta\sigma}{2} = \sigma_{\max} = \sigma'_f \cdot (2N_f)^b \quad (5)$$

In the previous two equations,  $\sigma'_f$  and  $b$  represents, respectively, the fatigue strength coefficient and exponent;  $\varepsilon'_f$  and  $c$  represents, respectively, the fatigue ductility coefficient and exponent and  $E$  is the Young modulus. The maximum stress,  $\sigma_{\max}$ , mean stress,  $\sigma_m$ , and the strain range,  $\Delta\varepsilon$  have to be evaluated as the average values at the elementary material block size,  $\rho^*$ , taking into account an elastoplastic analysis.

To compute the elastoplastic stresses and strains at the elementary material blocks ahead of the crack tip, Noroozi *et al.* [1,10] proposed the following analytical procedure:

- The elastic stresses are computed ahead of the crack tip, using the Creager-Paris solution [22] for a crack with a tip radius  $\rho^*$ , using the applied stress intensity factors.



- The actual elastoplastic stresses and strains, ahead of the crack tip, are computed using the Neuber [15] or Glinka's approaches [23]. Multiaxial approaches may be adopted using the procedures presented by Moftakhar *et al.* [16] and Reinhard *et al.* [17].
- The residual stress distribution ahead of the crack tip is computed using the actual elastoplastic stresses computed at the end of the first load reversal and subsequent cyclic elastoplastic stress range, along the y direction:

$$\sigma_r = \sigma_{\max} - \Delta\sigma \quad (6)$$

- The residual stress distribution computed ahead of the crack tip is assumed to be applied on crack faces, behind the crack tip, in a symmetric way with respect to the crack tip.
- The compressive stress distribution, acting on crack faces, is equivalent to a residual stress intensity factor which is used to correct the applied stress intensity factor range leading to a total (effective) stress intensity factor range, which excludes the effects of the compressive stresses. The residual stress intensity factor,  $K_r$ , is computed using the weight function method [24]:

$$K_r = \int_0^a \sigma_r(x) m(x, a) dx \quad (7)$$

where  $m(x, a)$  is the weight function [24] and  $\sigma_r(x)$  is the residual stress field computed from the elastoplastic stress analysis (see Eq. (6)).

- The applied stress intensity factors (maximum and range values) are then corrected using the residual stress intensity factor, resulting the total  $K_{\max, tot}$  and  $\Delta K_{tot}$  values [1,10]. For positive stress R-ratios, which is the range covered by the experimental data used in this research,  $K_{\max, tot}$  and  $\Delta K_{tot}$  may be computed as follows:

$$\begin{aligned} K_{\max, tot} &= K_{\max, applied} + K_r \\ \Delta K_{tot} &= \Delta K_{applied} + K_r \end{aligned} \quad (8)$$

where  $K_r$  assumes a negative value corresponding to the compressive stress field. For high stress R-ratios, the compressive stresses ahead of the crack tip may be neglected and the applied stress intensity factor range is assumed fully effective; for low stress R-ratios the compressive stresses increases and the effectiveness of the applied stress intensity factor range decreases accordingly.

- Using the total values of the stress intensity factors, the first and second steps before are repeated to determine the corrected values for the maximum actual stress and actual strain range at the material representative elements. Then, Eq. (2) is applied together with Eq. (1) to compute the fatigue crack growth rates.

The described methodology does not lead to close-form (explicit) solutions for the fatigue crack propagation rates. Nevertheless, adopting some simplified assumptions about the elastoplastic conditions, such as predominantly elastic behaviour of the material at the crack tip or predominantly plastic behaviour of the material at the crack tip, it is possible to derive those close-form solutions for the stress-strain histories at the crack tip and for the number of cycles to failure of the material representative element. In these cases, the fatigue crack propagation rates may be expressed in the following two-parameters crack driving relation [1, 10]:

$$\frac{da}{dN} = C \left[ (K_{\max, tot})^p (\Delta K_{tot})^q \right] \quad (9)$$

where  $C$ ,  $p$ ,  $q$  and  $\gamma$  are constants to be correlated with the cyclic constants of the material in a form depending on the elastoplastic conditions at the crack tip. This two-parameters ( $K_{\max}$  and  $\Delta K$ ) fatigue crack propagation relation allows the simulation of mean stress effects on fatigue crack propagation rates. The crack propagation models based on a two parameters crack driving force has been recently followed by several authors [25, 26].

### *Probabilistic $\epsilon$ -N and SWT-N fields*

The fatigue crack propagation modelling based on local approaches requires a fatigue damage relation to compute the number of cycles to fail the elementary material blocks. In this paper, probabilistic fatigue damage models are proposed rather than the deterministic *SWT-N*, Coffin-Manson or Morrow models often used in the literature. The probabilistic  $\epsilon$ -N model proposed by Castillo and Fernández-Canteli [20] is used. However, and since this probabilistic  $\epsilon$ -N model does not account for mean stress effects, an alternative probabilistic *SWT-N* field is also proposed, as an extension of the  $p$ - $\epsilon$ -N field suggested by Castillo and Fernández-Canteli [20], to account for mean stress effects.



Castillo and Fernández-Canteli [20] proposed a probabilistic model to describe the strain-life field of the material ( $p$ - $\varepsilon_a$ - $N$  field), based on Weibull distribution. The model assumes that the fatigue life,  $N_f$  and the total strain amplitude,  $\varepsilon_a$ , are random variables. Based on several physical and statistical considerations, such as the weakest link principle, stability, limit behaviour, range of the variables and compatibility, Castillo and Fernández-Canteli [20] derived a strain-life model, which shows exactly the same formulation as proposed the authors for the stress-life field. The interested readers can see the detailed assumptions in Castillo *et al.* [27, 28], where the stress version of the model has been studied and successfully applied to different cases of lifetime problems. This leads to the Weibull strain-life model [28]:

$$p = F(N_f^*; \varepsilon_a^*) = 1 - \exp \left\{ - \left[ \frac{\log(N_f/N_0) \log(\varepsilon_a/\varepsilon_{a0}) - \lambda}{\delta} \right]^\beta \right\} \quad (10)$$

$$\log(N_f/N_0) \log(\varepsilon_a/\varepsilon_{a0}) \geq \lambda$$

where  $p$  is the probability of failure,  $N_0$  and  $\varepsilon_{a0}$  are normalizing values, and  $\lambda$ ,  $\delta$  and  $\beta$  are the non-dimensional Weibull model parameters. Their physical meanings (see Fig. 2) are:

- $N_0$ : Threshold value of lifetime;
- $\varepsilon_{a0}$ : Endurance limit of  $\varepsilon_a$ ;
- $\lambda$ : Parameter defining the position of the corresponding zero-percentile curve;
- $\delta$ : Scale parameter;
- $\beta$ : Shape parameter.

Note that the strain-life model (Eq. (10)) has a dimensionless form and reveals that the probability of failure  $p$  depends only on the product  $N_f^* \varepsilon_a^*$ , where  $N_f^* = \log(N_f/N_0)$  and  $\varepsilon_a^* = \log(\varepsilon_a/\varepsilon_{a0})$ , that is:

$$N_f^* \varepsilon_a^* \sim W(\lambda, \delta, \beta) \Leftrightarrow N_f^* \sim W\left(\frac{\lambda}{\varepsilon_a^*}, \frac{\delta}{\varepsilon_a^*}, \beta\right) \quad (11)$$

i.e.,  $N_f^* \varepsilon_a^*$  has a Weibull distribution.

This model provides a complete analytical description of the statistical properties of the physical problem being dealt with, including the quantile curves without the need of separating the total strain in its elastic and plastic components but dealing with the total strains directly [20]. With respect to the conventional Coffin-Manson approach, the strain-life probabilistic model show some advantages: it arises from sound statistical and physical assumptions and not from an empirical arbitrary assumption; it provides a probabilistic definition of the whole strain-life field; it does not need to consider separately the elastic and the plastic strains; the run-outs can also be used in the analysis, and facilitates damage analysis.

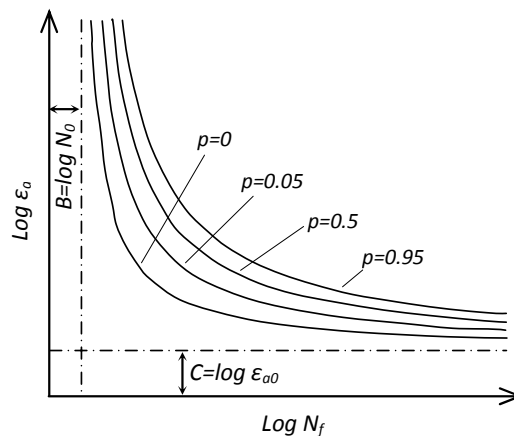


Figure 2: Percentile curves representing the relationship between dimensionless lifetime,  $N_f^*$ , and the strain amplitude,  $\varepsilon_a^*$ :  $p$ - $\varepsilon_a$ - $N$  field.

The  $SWT$  ( $=\sigma_{max} \cdot \varepsilon_a$ ) parameter was proposed by Smith *et al.* [8] in order to account for mean stress effects on fatigue life prediction. Any combination of maximum stress and strain amplitude that leads to the same  $SWT$  parameter should lead



to the same fatigue life. The  $SWT-N$  and  $\varepsilon_a-N$  fields exhibit similar characteristics. Therefore the  $p-\varepsilon-N$  field proposed by Castillo and Fernández-Canteli [20] may be extended to represent the  $p-SWT-N$  field as:

$$p = F(N_f^*; SWT^*) = 1 - \exp \left\{ - \left[ \frac{\log(N_f/N_0) \log(SWT/SWT_0) - \lambda}{\delta} \right]^\beta \right\} \quad (12)$$

$$\log(N_f/N_0) \log(SWT/SWT_0) \geq \lambda$$

where  $p$  is the probability of failure,  $N_0$  and  $SWT_0$  are normalizing values, and  $\lambda$ ,  $\delta$  and  $\beta$  are the non-dimensional Weibull model parameters. Similarly to the  $p-\varepsilon-N$  field, the physical meaning of the parameters from Eq. (12) (see Fig. 3) are:

$N_0$ : Threshold value of lifetime;

$SWT_0$ : fatigue limit of  $SWT$ ;

$\lambda$ ,  $\delta$  and  $\beta$ : Weibull distribution parameters.

Eq. (12) has also a dimensionless form and reveals that the probability of failure  $p$  depends only on the  $N_f^* SWT^*$  product, where  $N_f^* = \log(N_f/N_0)$  and  $SWT^* = \log(SWT/SWT_0)$  that is:

$$N_f^* SWT^* \sim W(\lambda, \delta, \beta) \Leftrightarrow N_f^* \sim W\left(\frac{\lambda}{SWT^*}, \frac{\delta}{SWT^*}, \beta\right) \quad (13)$$

i.e.,  $N_f^* SWT^*$  follows a Weibull distribution.

The parameters  $\log N_0$  and  $\log \varepsilon_{a0}$  of the  $p-\varepsilon_a-N$  model,  $\log N_0$  and  $\log SWT_0$  of the  $p-SWT-N$  model can be estimated by least square method. The Weibull parameters can be estimated using the maximum likelihood method [27, 28].

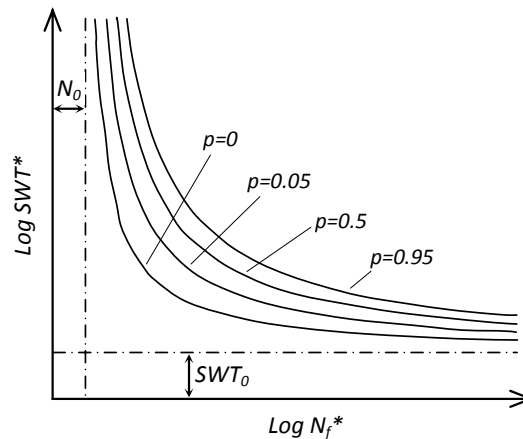


Figure 3: Percentile curves representing the relationship between dimensionless lifetime,  $N_f^*$ , and the  $SWT^*$  damage parameter:  $p-SWT-N_f$  field.

## PROCEDURE TO GENERATE PROBABILISTIC FATIGUE CRACK PROPAGATION FIELDS

The procedure proposed to derive probabilistic fatigue crack propagation fields may be summarized into the following steps:

- 1) Estimation of the Weibull parameters for the  $p-SWT-N$  or  $p-\varepsilon_a-N$  fields, using experimental  $\varepsilon_a-N$  or  $SWT-N$  data from smooth specimens;
- 2) Application of the UniGrow model together with the probabilistic fatigue damage models;
- 3) Computation of the  $p-da/dN-AK-R$  fields.

The UniGrow model was implemented in a worksheet, supported on VBA programming, specifically developed for Compact Tension (CT) specimens. The input data are the material properties, loads, dimensions of the CT specimen, including the initial and final crack size to be simulated. Additionally, the elementary material block size,  $\varrho^*$ , is required. This parameter may be evaluated by a trial and error procedure in order the numerical results fit satisfactorily the



experimental data. Fig. 4 gives a general overview of the procedure. The probabilistic fatigue crack propagation fields were evaluated using, alternatively, the probabilistic  $\varepsilon$ - $N$  and  $SWT$ - $N$  fields. The residual stress fields ahead of the crack tip were evaluated in this paper using an elastoplastic finite element model of the CT specimens.

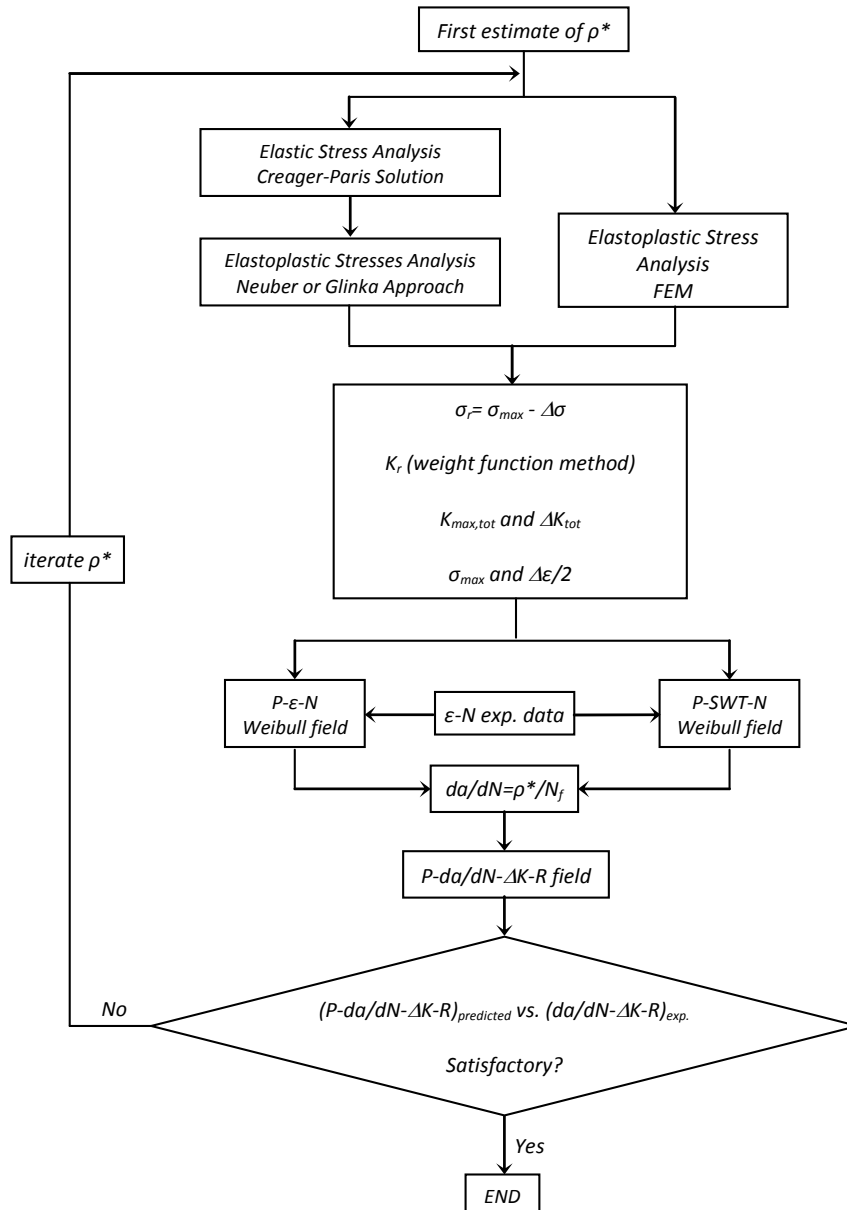


Figure 4: Procedure to generate probabilistic fatigue crack propagation fields.

## EXPERIMENTAL FATIGUE DATA OF THE S355 MILD STEEL

The fatigue behaviour of the S355 mid steel was evaluated by De Jesus *et al.* [19], based on experimental results from fatigue tests of smooth specimens and fatigue crack propagation tests. The fatigue tests of smooth specimens were carried out according to the ASTM E606 standard [29], under strain-controlled conditions. Tab. 1 and 2 summarize the elastic ( $E$ : Young modulus) and monotonic strength properties ( $f_y$ : yield strength;  $f_u$ : tensile strength) as well as the cyclic elastoplastic constants ( $K'$ : cyclic strain hardening coefficient;  $n'$ : cyclic strain hardening exponent) and the strain-life constants (refer to Eq. (3)–(5)). The crack propagation tests were performed using compact tension (CT) specimens, according to the procedures of the ASTM E647 standard [30], under load-controlled conditions. Fig. 5



presents the experimental fatigue crack propagation rates obtained for the S355 steel, where stress ratio effects on fatigue crack propagation rates are shown. An increase in fatigue crack propagation rates is clear, when the stress ratio changes from 0 to any positive stress ratios considered in the experimental program. Also, it is clear that all the positive stress ratios resulted in similar crack propagation rates. This behaviour is consistent with a crack closure effect that occurs between  $R_\sigma=0.0$  and  $R_\sigma=0.25$ . For  $R_\sigma=0.0$  there is some crack closure, the applied stress intensity factor range being not fully effective. For  $R_\sigma=0.25$  and higher, there is no crack closure, the applied stress intensity factor range being fully effective. Details about the properties evaluation for the S355 steel can be found in reference [19].

E [GPa]	$f_u$ [MPa]	$f_y$ [MPa]	$K'$ [MPa]	$n'$
211.60	744.80	422.00	595.85	0.0757

Table 1: Monotonic and cyclic elastoplastic properties of the S355 mid steel.

$\sigma'_f$ [MPa]	$b$	$\epsilon'_f$	$c$
952.20	-0.0890	0.7371	-0.6640

Table 2: Morrow constants of the S355 mid steel.

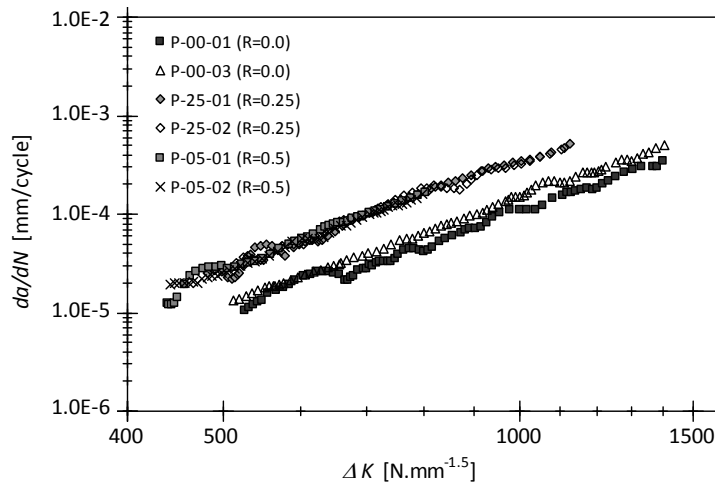


Figure 5: Experimental fatigue crack propagation data of the S355 steel for distinct stress ratios: experimental results.

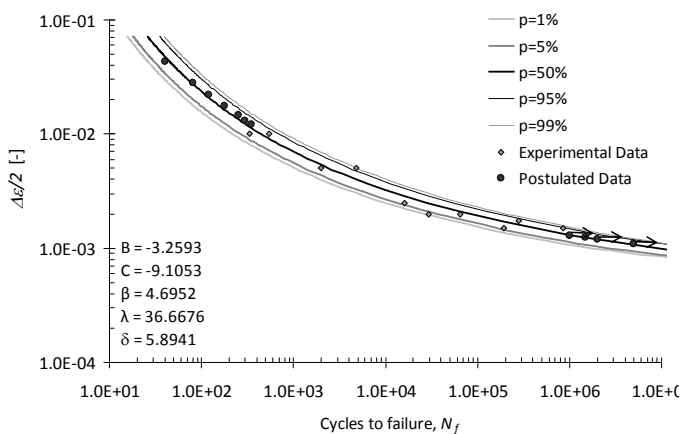


Figure 6:  $p$ - $\epsilon$ - $N$  field for the S355 steel.

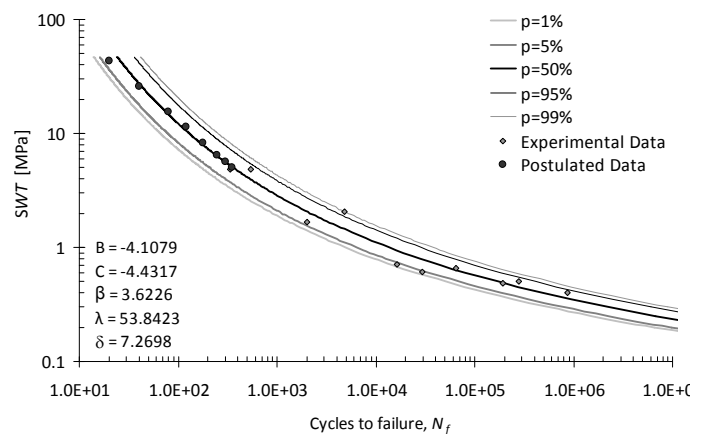


Figure 7:  $p$ - $SWT$ - $N$  field for the S355 steel.

The  $p$ - $\epsilon$ - $N$  and  $p$ - $SWT$ - $N$  fields of the S355 steel are presented in Figs. 6 and 7, respectively. The constants of the Weibull fields are also referred in the figures. The extrapolations using the Weibull field should be avoided for high- and low-cycle fatigue lives. Since the number of cycles to fail the representative volume element, in the crack propagation regime, may



be low, it was decided to postulate some fatigue data at the low- to very low-cycle fatigue domain, using the Morrow equation of the material, for that purpose. The Morrow equation is more reliable to perform extrapolations for very low number of cycles than the Weibull field since the Weibull field shows an abnormal asymptotic behaviour for very low-cycle fatigue.

## PROBABILISTIC FATIGUE CRACK PROPAGATION RATES PREDICTIONS

The probabilistic fatigue crack propagation rates predictions were based on the application of the UniGrow model to the CT specimens. The elementary material block size,  $\rho^*$ , is required. A trial and error procedure was adopted in order to result a good agreement between the numerical and experimental  $da/dN$  vs.  $\Delta K$  data, for the materials under consideration (see Fig. 4). The probabilistic fatigue crack propagation fields were evaluated using both the probabilistic  $\varepsilon_r-N$  and  $SWT-N$  fields, for comparison purposes. The procedure to generate the probabilistic fatigue crack propagation fields was aforementioned and illustrated in the Fig. 5.

### *Finite element analysis of the CT geometry*

In order to assess the accuracy of the simplified elastoplastic analysis proposed in the Unigrow model for the residual stress estimation, a bi-dimensional parametric finite element model of the CT specimen was built and used in an elastoplastic finite analysis, using ANSYS® 12.0 commercial code [31]. Fig. 8 illustrates the typical finite element mesh of the CT geometry with the respective boundary conditions.

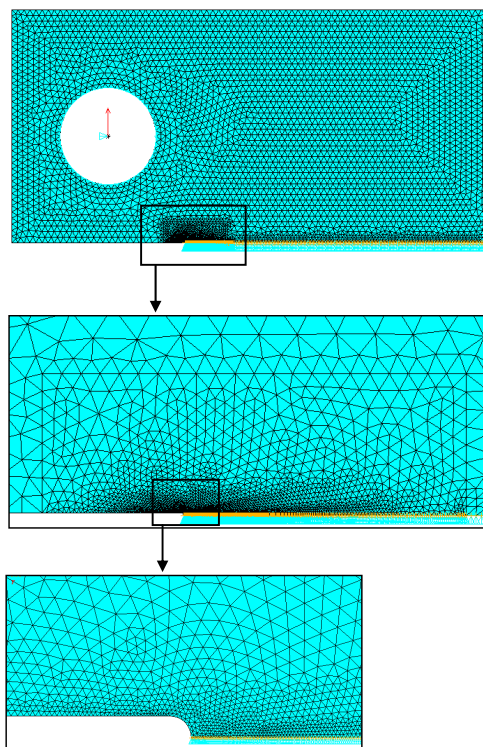


Figure 8: Typical finite element mesh of the CT specimen, using 6-noded quadratic triangular plane stress elements.

Only  $\frac{1}{2}$  of the geometry is modelled, taking into account the existing plane of symmetry. Plane stress conditions were assumed since the thickness of specimens are relatively reduced ( $B=8\text{mm}$ ). Plane stress quadratic 6-noded triangular elements were used in the analysis (SOLID183), with 3 integration points. In order to simulate the pin loading, rigid-to-flexible contact was used with a friction coefficient,  $\mu=0.3$ . The pin was modelled as a rigid circle controlled by a pilot node, using TARGE169 elements. The surface of the holes was modelled as a flexible surface using CONTA172 elements. The Augmented Lagrange contact algorithm was used. The associative Von Mises (J2) yield theory with multilinear kinematic hardening was used to model the plastic behaviour. Fig. 9 shows the superposition of the Ramberg-Osgood relation [32] with the response of a finite element model reproducing a uniaxial stress state (single cubic element



model). Besides the symmetry boundary conditions, the pilot node controlling the pin displacement was restricted along the loading direction. Finally, the load was applied directly to the pilot node. It is interesting to note that the crack was modelled with a tip radius of  $\varrho^*$ , according the assumptions of Fig. 1b. The mesh size at crack tip was calibrated using a convergence study taking into account the elastic stresses along the crack plane ( $\sigma_x$ : crack plane direction;  $\sigma_y$ : crack plane normal direction). Fig. 10 illustrates the crack tip meshes considered in this convergence study and mesh 2 was the one adopted for the numerical simulations. Tab. 3 presents the maximum elastic stresses ( $\sigma_x$  and  $\sigma_y$ ) ahead of the crack tip, resulting from distinct mesh densities, for the S355 steel. The results are compared between the adopted reference mesh 2 and the other tested meshes. Mesh 2 gives a good compromise between computational cost and stability of the solution.

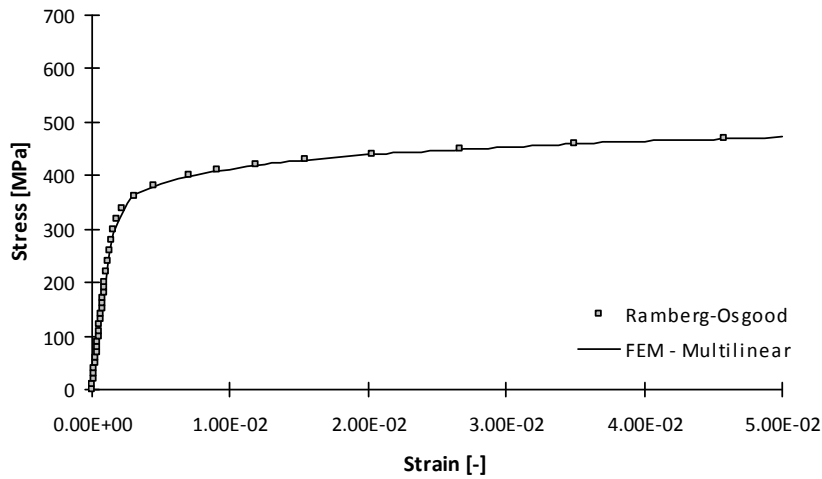


Figure 9: Cyclic curve of the S355 steel.

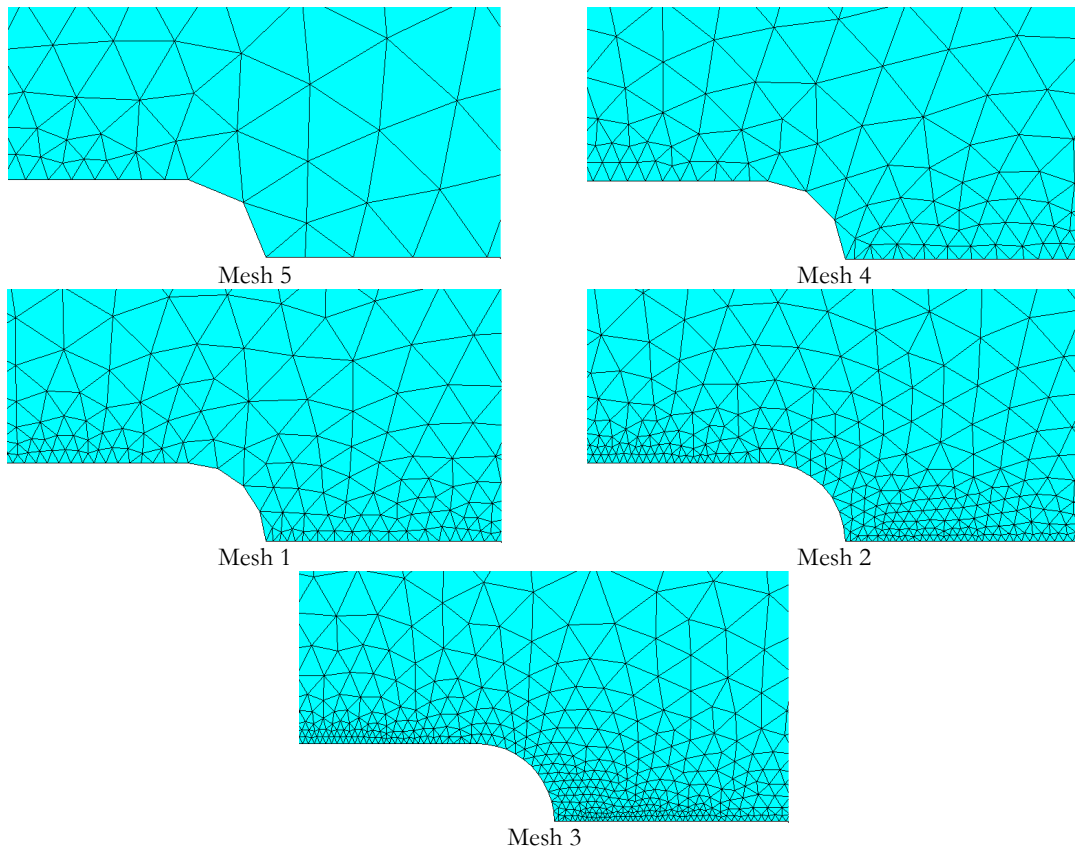


Figure 10: Finite element meshes used in the convergence study for the S355 steel ( $\varrho^*=55\mu\text{m}$ ).

Maximum stress	mesh 5	mesh 4	mesh 1	mesh 2	mesh 3
$\sigma_y$ [MPa]	1637.00	1772.00	1797.00	1926.90	1928.80
Dev. [%]	-15.04	-9.04	-6.71	-	0.10
$\sigma_x$ [MPa]	419.70	423.83	416.67	417.89	417.78
Dev. [%]	2.83	1.42	-0.29	-	-0.03

Table 3: Maximum elastic stresses for distinct finite element mesh densities for the S355 steel ( $F_{max}=5443.5N$ ,  $a=10mm$ ,  $\rho^*=55\mu m$ ).

The finite element model was used to simulate a loading and unloading sequence. The residual stresses are computed from the stress field at the end of the unloading load step. Alternatively, the simplified analytical solution based on multiaxial Neuber’s approach [15] was implemented for comparison purposes. In this case, the residual stresses resulted from the subtraction of the cyclic elastoplastic stress range to the maximum elastoplastic stress, both computed in an independent way. The finite element model was initially applied to perform elastic and elastoplastic stress analyses in order to allow the comparison of the elastic and elastoplastic stress distributions, respectively with the Creager-Paris solution [22] and multiaxial Neuber’s approach [15]. According to the UniGrow model, the compressive residual stresses computed ahead the crack tip are assumed to be applied symmetrically, in the crack faces. Using the weight function method [24], the residual stress intensity factor,  $K_r$ , was computed for the stress  $R$ -ratios considered in the experimental program. The elastic stress distributions from the numerical and analytical solutions for the CT specimens made of the S355 steel are compared in Fig. 11. Fig. 12 compares the elastoplastic stress distributions. The results were computed for a crack tip radius,  $\rho^*=5.5\times 10^{-5}m$ , which was found to be the best value for the S355 steel, that gives the best predictions for the crack growth rates, based on  $SWT$  fatigue damage probabilistic field.

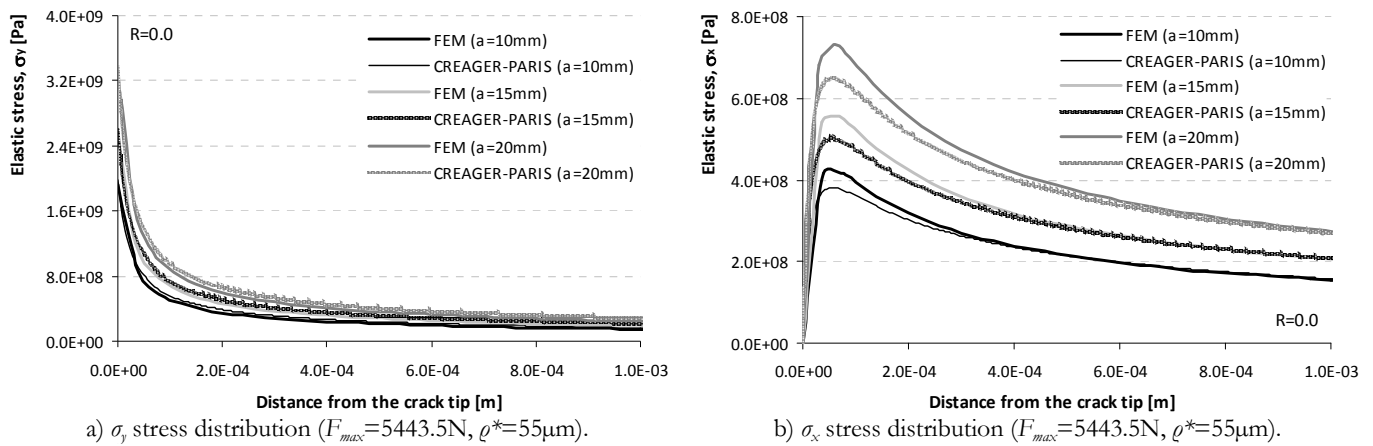


Figure 11: Elastic stress distribution ahead of the crack tip and along the crack plane line ( $y=0$ ) for CT specimens made of the S355 steel: comparison between analytical and numerical results. Distinct crack sizes considered.

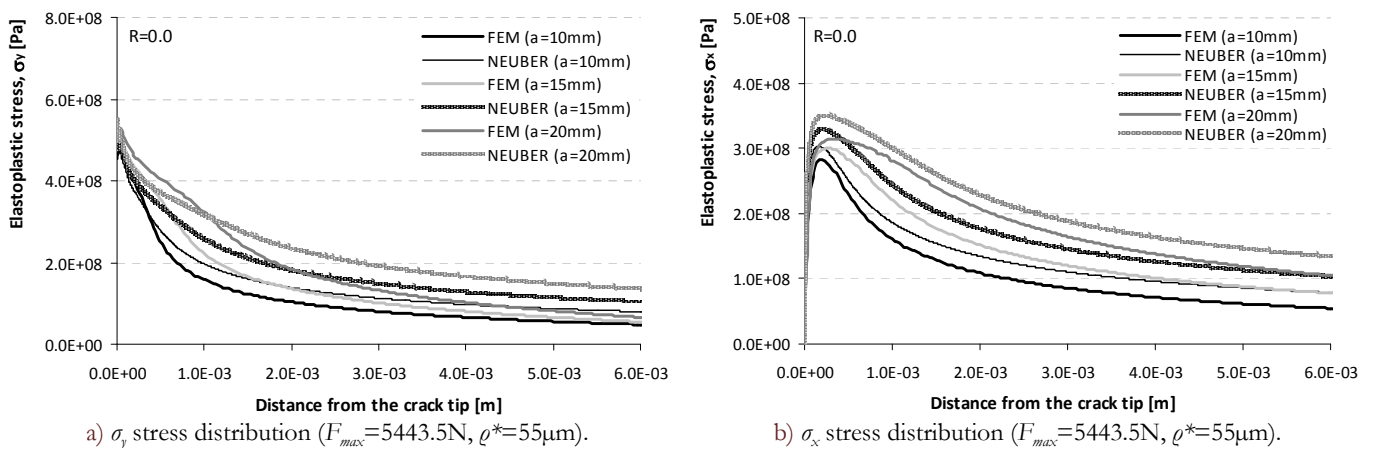


Figure 12: Elastoplastic stress distribution ahead of the crack tip along the crack plane line ( $y=0$ ) for CT specimens made of S355 steel: comparison between analytical and numerical results. Distinct crack sizes considered.



The residual stress distributions are illustrated in Fig. 13, for distinct crack sizes and stress R-ratios, for the CT specimens made of S355 steel and assuming  $\rho^*=5.5\times 10^{-5}\text{m}$ . These residual stresses were computed using both analytical and numerical solutions.

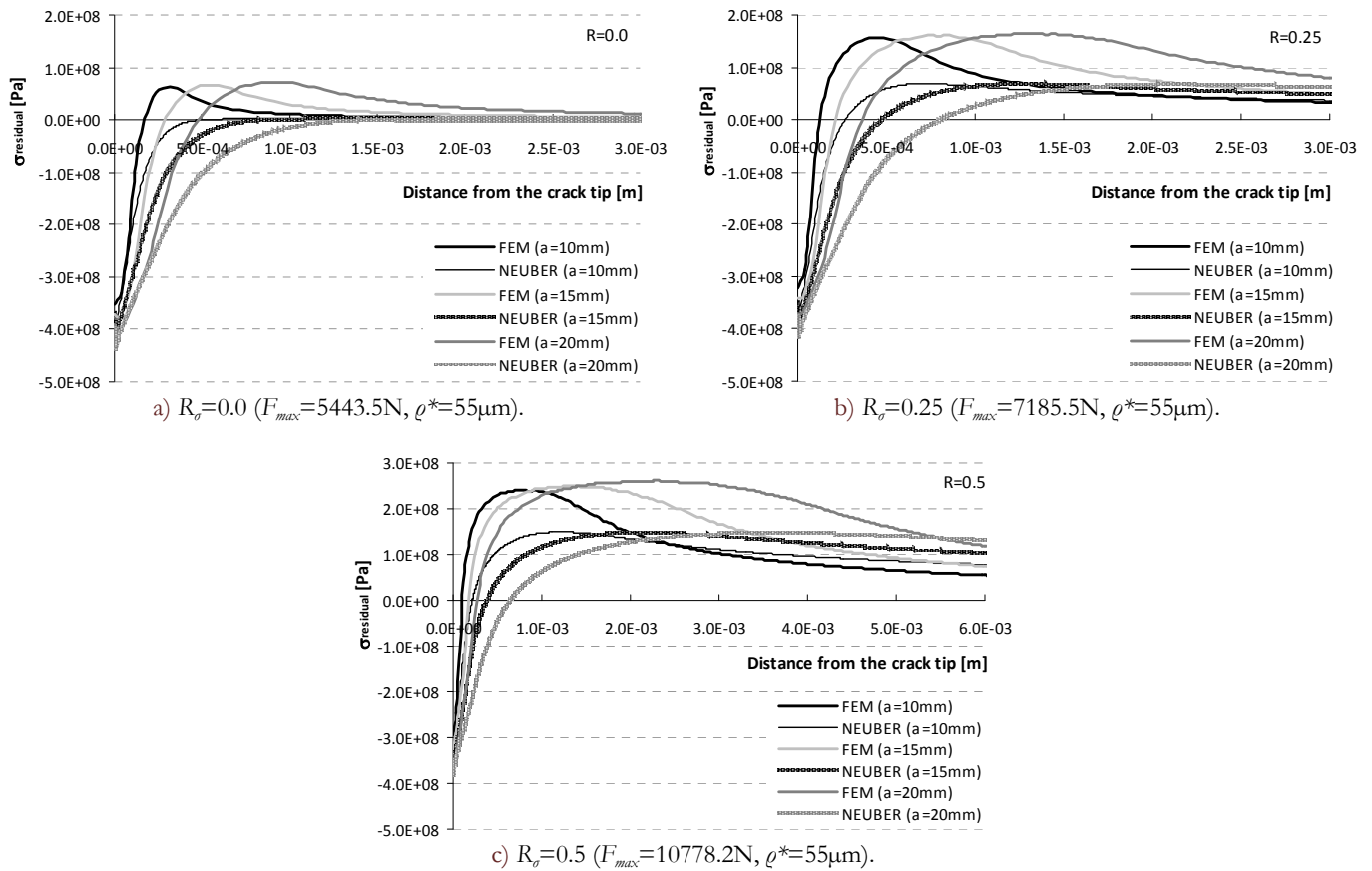


Figure 13: Residual stress distribution ahead of the crack tip along the crack plane line ( $y=0$ ) for CT specimens made of S355 steel: comparison between analytical and numerical results. Distinct stress ratios and crack sizes considered.

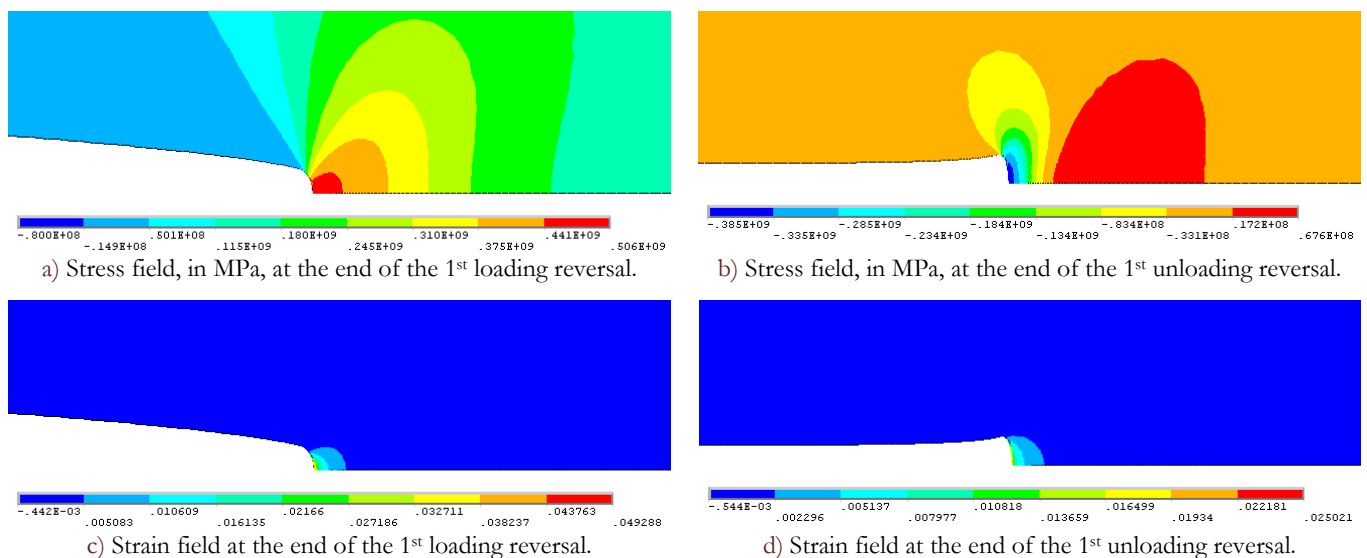


Figure 14: Stress and strain fields, along the load direction, obtained for the CT specimens made of S355 steel, resulting from elastoplastic finite element analysis ( $\rho^*=55\mu\text{m}$ ,  $a=15\text{mm}$ ,  $R_\sigma=0.0$ ,  $F_{max}=5443.5\text{N}$ ).

The stress and strain fields along the  $y$  (load) direction assuming a material representative element of  $\rho^*=55\mu\text{m}$ , a crack size  $a=15\text{mm}$ , a maximum load  $F_{max}=5443.5\text{N}$ , and a stress R-ratio,  $R_p=0.0$ , obtained for the CT specimens using the elastoplastic finite element analysis, are illustrated in Fig. 14. It is clear the compressive stress field at the crack tip vicinity and at some extension of the crack wake. The stress and strain fields are shown at the end of the first loading reversal and at the end of the unloading reversal.

Fig. 15 presents the residual stress intensity factor as a function of the applied stress intensity factor range obtained for the CT specimens made of S355 steel, using the numerical analysis.

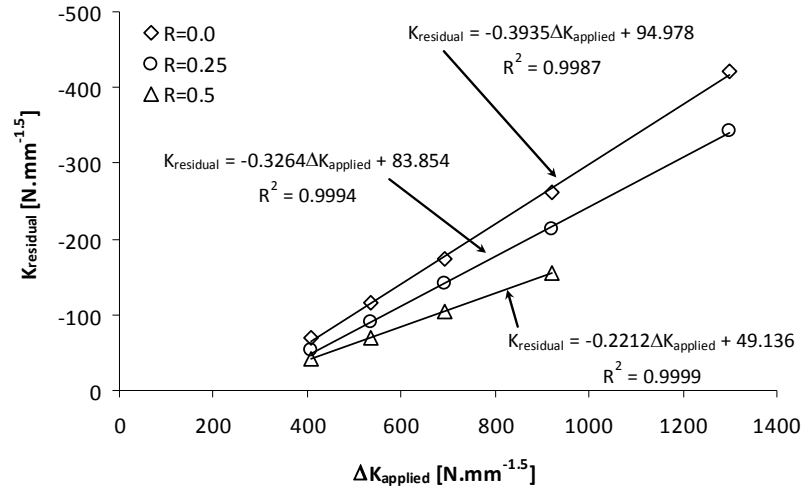


Figure 15: Residual stress intensity factor as a function of the applied stress intensity factor range obtained for the S355 steel ( $\rho^*=5.5\times 10^{-5}\text{m}$ ).

The elastic stress distributions presented a satisfactory agreement between the analytical and numerical results, for several crack sizes (measured from loading line), within a small distance from the crack tip. For higher distances, slight deviations are found for  $\sigma_y$  stresses. For  $\sigma_x$  stresses, the maximum deviation is found in the maximum absolute value. For small and high distances from the crack tip, the deviations on  $\sigma_x$  stresses are minimal. Additional simulations with further mesh refinements did not produce noticeable changes in the elastic stress distributions, demonstrating a good mesh refinement. Besides the numerical solution for the elastoplastic analysis, results from the multiaxial Neuber's analysis are also considered. Despite the same global trends are observed for the  $\sigma_y$  and  $\sigma_x$  stress distributions, deviations in maximum absolute values are verified in the elastoplastic stresses. In general, the analytical solutions lead to maximum absolute stresses higher than the elastoplastic FE analysis.  $\sigma_x$  stresses are more stepped than the corresponding numerical stresses near the crack tip. Also, the analytical solution shows some instability near the crack tip. The analysis of the  $\sigma_y$  stress distribution shows an inflection point which is related to the size of the plastic zone. The analytical solution does not show this behaviour, which is a clear limitation of the analytical approach.

The compressive residual stresses decrease progressively with increasing stress ratio, making the applied stress intensity range more effective. The extension of the compressive residual stresses increases with the crack size. The numerical model always predicts a compressive stress region which is lower than that predicted using the analytical model. The comparison between the numerical and analytical results highlighted some inconsistencies in the analytical results. The analytical procedure produces reliable results at the crack notch root, but the residual stress distribution along the crack front path (away from the crack notch root) seems to be inconsistent, which is in part justified by the incapacity of the analytical model to handle the stress redistribution due to yielding. Therefore, the numerical solution, for the residual stresses, was adopted in the crack propagation prediction, based on the UniGrow model.

A linear correlation between the residual stress intensity factor and the applied stress range is verified, for each stress R-ratio. This linear relation agrees with the proposition by Noroozi *et al.* [10].

#### *p-da/dN-ΔK-R results and discussion*

The UniGrow model was applied to compute the fatigue crack propagation for the same experimental conditions used to derive the aforementioned fatigue crack propagation data. The residual stress intensity factor was computed based on compressive residual stress distribution from the finite element analysis, and using the weight function method [24], as proposed in the UniGrow model. The strain range and maximum stress required by the probabilistic *strain-life* or *SWT-life*



models were assessed using the analytical approach, applied to the first elementary material block, keeping the original structure of the UniGrow model. Average strain and stress values, along the first elementary material block, were used instead of peak values. The analytical solution produces reliable results at the crack tip notch root as verified in previous section. The original structure of the UniGrow model has some advantages:

- i) a direct correspondence with fracture mechanics based analyses, which facilitates the physical understanding of the process;
- ii) allows close form solutions for fatigue crack propagation laws in the same format of existing fracture mechanics approaches;
- iii) requires inexpensive computations.

The elastoplastic finite element analysis was used for the derivation of the residual stresses which were afterwards used for the computation of the residual stress intensity factor, using the weight function method.

The  $p$ - $SWT$ - $N$  or the  $p$ - $\varepsilon_a$ - $N$  fields were used to derive the probabilistic fatigue crack propagation fields ( $p$ - $da/dN$ - $\Delta K$ - $R$  fields). For each case, an independent identification of the elementary material block size,  $\varrho^*$ , was performed. Fig. 16 shows the probabilistic fatigue crack propagation fields that were obtained, for the S355 steel, using the  $p$ - $\varepsilon_a$ - $N$  field. Fig. 17 illustrates the probabilistic fatigue crack propagation fields predicted for the S355 steel, resulting from the  $p$ - $SWT$ - $N$  field. An elementary material block size of  $5.5 \times 10^{-5}$  m was found suitable for both  $p$ - $SWT$ - $N$  and  $p$ - $\varepsilon_a$ - $N$  damage fields. Concerning the  $p$ - $da/dN$ - $\Delta K$ - $R$  fields predicted for the S355 steel, the field that resulted from the  $p$ - $SWT$ - $N$  damage model produced the best results. This observation is justified by the fact that the S355 steel shows a markedly stress ratio influence on fatigue crack propagation rates, requiring a fatigue damage model that is able to account for the mean stress effects.

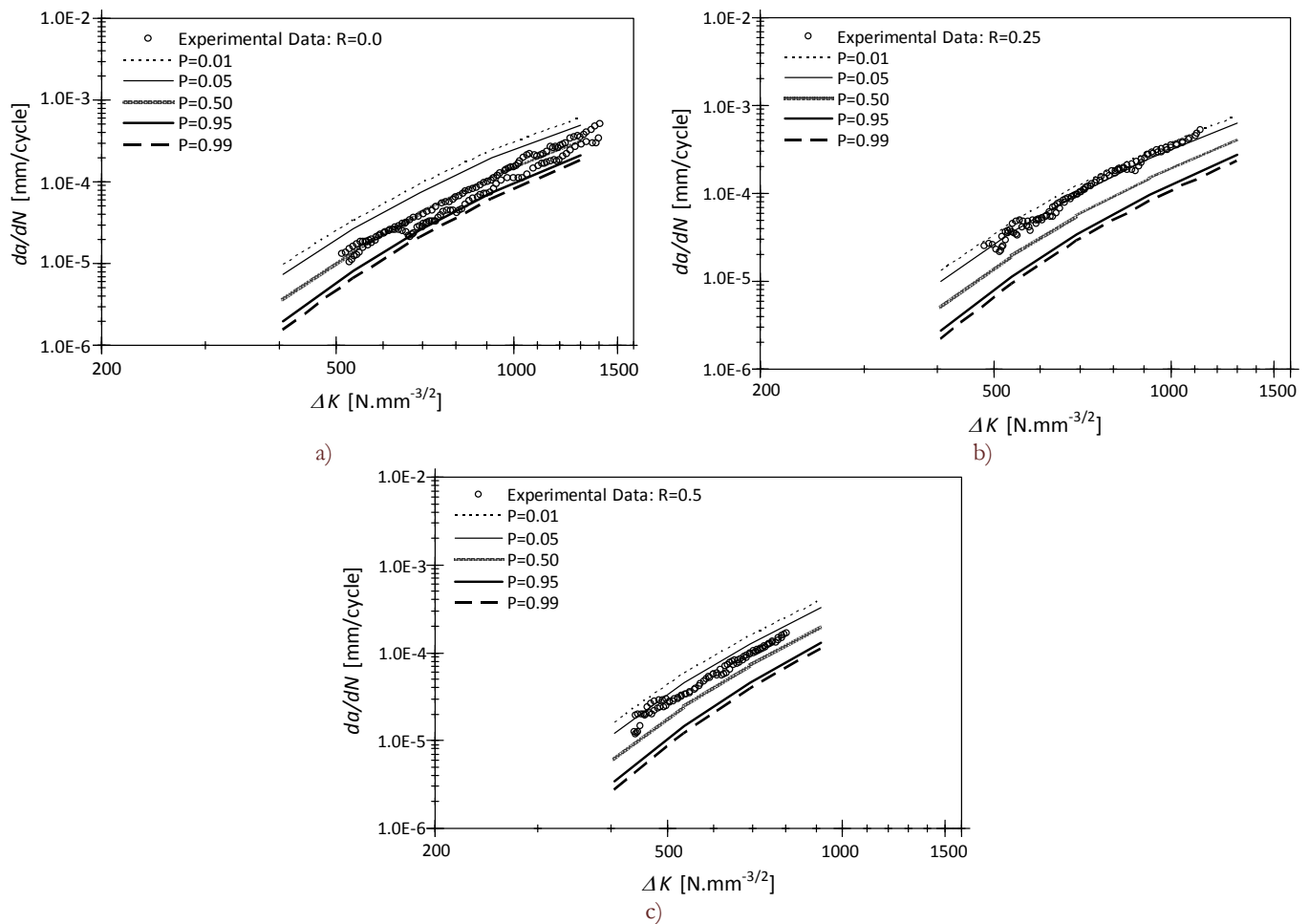


Figure 16: Probabilistic prediction of the fatigue crack propagation based the  $p$ - $\varepsilon$ - $N$  field, for the S355 steel: a)  $R_\sigma=0$ ; b)  $R_\sigma=0.25$ ; c)  $R_\sigma=0.5$ .

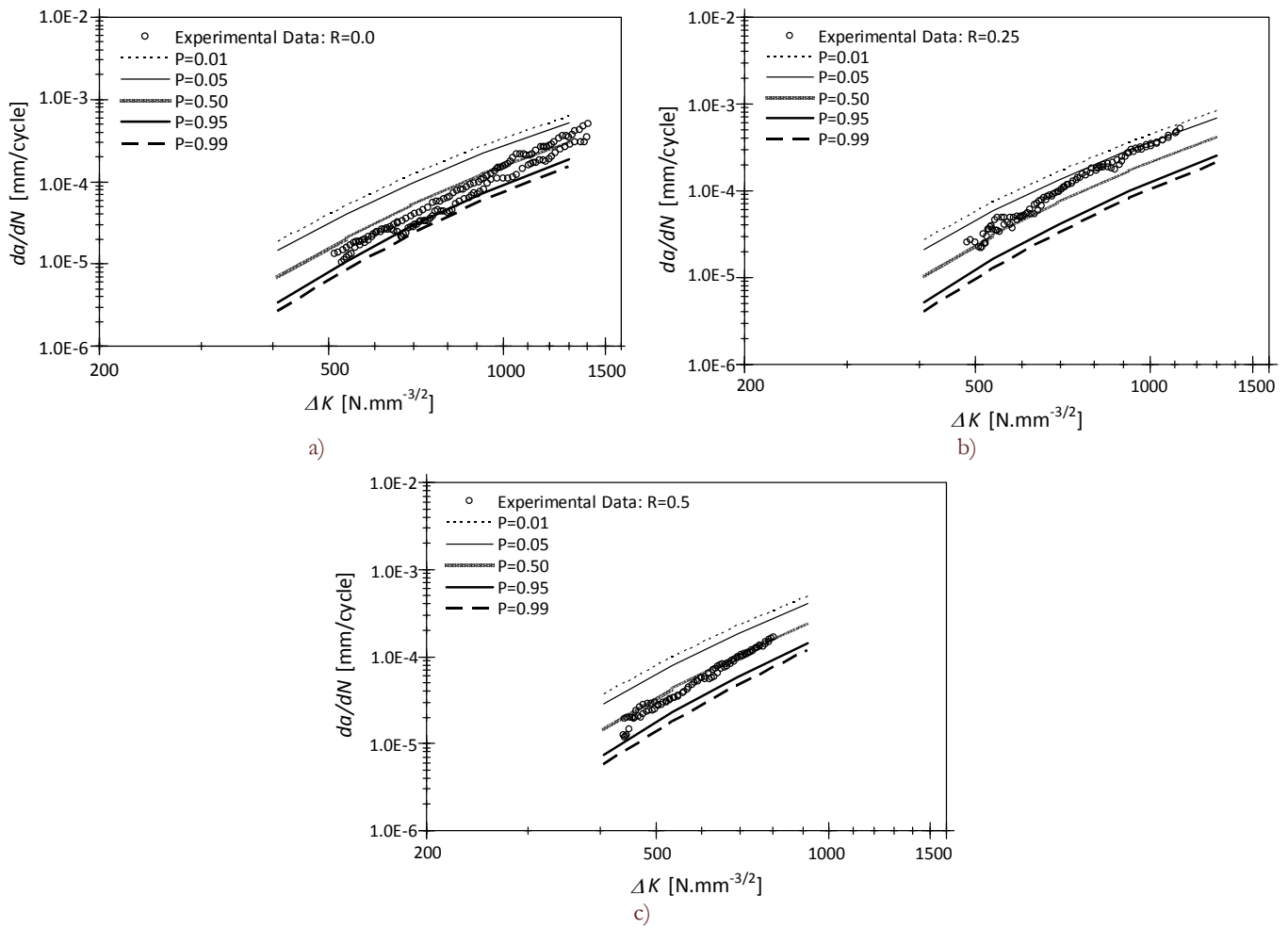


Figure 17: Probabilistic prediction of the fatigue crack propagation based on the  $p$ - $SWT$ - $N$  field, for the S355 steel: a)  $R_\sigma=0$ ; b)  $R_\sigma=0.25$ ; c)  $R_\sigma=0.5$ .

## CONCLUSIONS

An assessment of the UniGrow model was presented in this paper, based on available experimental data for the S355 mild steel. The UniGrow model was also extended to predict probabilistic fatigue crack propagation fields, replacing the deterministic  $SWT$ - $N$  relation proposed in the UniGrow model by  $p$ - $SWT$ - $N$  or  $p$ - $\varepsilon_a$ - $N$  fields. The  $p$ - $SWT$ - $N$  field was firstly proposed in the present paper, as a generalization of the  $p$ - $\varepsilon_a$ - $N$  field, in order to take into account the mean stress effects. Elastoplastic finite element analysis was used to compute the residual stress field which is a more accurate than using the analytical elastoplastic formulae that does not account for stress redistribution due to yielding. The predicted  $p$ - $da/dN$ - $\Delta K$ - $R$  field for the S355 steel, based on the material  $p$ - $SWT$ - $N$  field, showed a satisfactory agreement with the available experimental data. The proposed  $p$ - $da/dN$ - $\Delta K$ - $R$  fields were able to model conveniently the stress  $R$ -ratio effects on crack propagation rates as well as to represent the scatter on these fatigue crack propagation rates. The elementary material block size found for the material is within the same order of magnitude for this parameter found by Noroozi *et al.* [10].

## ACKNOWLEDGEMENTS

The authors acknowledge the Portuguese Science Foundation (FCT) for the financial support through the doctoral grant SFRH/BD/66497/2009.



## REFERENCES

- [1] Noroozi, A.H., Glinka, G., Lambert, S., A two parameter driving force for fatigue crack growth analysis, *International Journal of Fatigue*, 27 (2005)1277-1296.
- [2] Schütz, W., A History of Fatigue, *Engineering Fracture Mechanics*, 54 (1996) 263-300.
- [3] Paris, P.C., Gomez, M., Anderson, W.E., A rational analytic theory of fatigue, *Trend Engineering*, 13 (1961) 9-14.
- [4] Beden, S.M., Abdullah, S., Ariffin, A.K., Review of Fatigue Crack Propagation Models for Metallic Components, *European Journal of Scientific Research*, 28 (2009) 364-397.
- [5] Coffin, L.F., A study of the effects of the cyclic thermal stresses on a ductile metal, *Translations of the ASME*, 76 (1954) 931-950.
- [6] Manson, S.S., Behaviour of materials under conditions of thermal stress, NACA TN-2933, National Advisory Committee for Aeronautics, (1954).
- [7] Morrow, J.D., Cyclic plastic strain energy and fatigue of metals, *Int. Friction, Damping and Cyclic Plasticity*, ASTM STP 378, (1965) 45-87.
- [8] Smith, K.N., Watson, P., Topper, T.H., A Stress-Strain Function for the Fatigue of Metals, *Journal of Materials*, 5(4) (1970) 767-778.
- [9] Shang, D.-G., Wang, D.-K., Li, M., Yao, W.-X., Local stress–strain field intensity approach to fatigue life prediction under random cyclic loading, *International Journal of Fatigue*, 23 (2001) 903–910.
- [10] Noroozi, A.H., Glinka, G., Lambert, S., A study of the stress ratio effects on fatigue crack growth using the unified two-parameter fatigue crack growth driving force, *International Journal of Fatigue*, 29 (2007) 1616-1633.
- [11] Noroozi, A.H., Glinka, G., Lambert, S., Prediction of fatigue crack growth under constant amplitude loading and a single overload based on elasto-plastic crack tip stresses and strains, *Engineering Fracture Mechanics*, 75 (2008) 188-206.
- [12] Pecker, E., Niemi, E., Fatigue crack propagation model based on a local strain approach, *Journal of Constructional Steel Research*, 49 (1999) 139–155.
- [13] Glinka, G., A notch stress-strain analysis approach to fatigue crack growth, *Engineering Fracture Mechanics*, 21 (1985) 245-261.
- [14] Hurley, P.J., Evans, W.J., A methodology for predicting fatigue crack propagation rates in titanium based on damage accumulation, *Scripta Materialia*, 56 (2007) 681–684.
- [15] Neuber, H., Theory of stress concentration for shear-strained prismatic bodies with arbitrary nonlinear stress–strain law, *Trans. ASME Journal of Applied Mechanics*, 28 (1961) 544–551.
- [16] Moftakhar, A., Buczynski, A., Glinka, G., Calculation of elasto-plastic strains and stresses in notches under multiaxial loading, *International Journal of Fracture*, 70 (1995) 357-373.
- [17] Reinhard, W., Moftakhar, A., Glinka, G., An Efficient Method for Calculating Multiaxial Elasto-Plastic Notch Tip Strains and Stresses under Proportional Loading, *Fatigue and Fracture Mechanics*, ASTM STP 1296, R.S. Piascik, J.C. Newman, N.E. Dowling, Eds., American Society for Testing and Materials, 27 (1997) 613-629.
- [18] Mikheevskiy, S., Glinka, G., Elastic–plastic fatigue crack growth analysis under variable amplitude loading spectra,” *International Journal of Fatigue*, 31 (2009) 1828–1836.
- [19] De Jesus, A.M.P., Matos, R., Fontoura, B.F.C., Rebelo, C., Simões da Silva, L., Veljkovic, M., A comparison of the fatigue behavior between S355 and S690 steel grades, *Journal of Constructional Steel Research*, 79 (2012) 140–150.
- [20] Castillo, E., Fernández-Canteli, A., *A Unified Statistical Methodology for Modeling Fatigue Damage*, Springer, (2009).
- [21] Basquin, O.H., The exponential law of endurance tests, In: *Proc. Annual Meeting, American Society for Testing Materials*, 10 (1910) 625-630.
- [22] Creager, M., Paris, P.C., Elastic field equations for blunt cracks with reference to stress corrosion cracking, *International Journal of Fracture Mechanics*, 3 (1967) 247–252.
- [23] Molski, K., Glinka, G., A method of elastic-plastic stress and strain calculation at a notch root, *Materials Science and Engineering*, 50 (1981) 93-100.
- [24] Glinka, G., Development of weight functions and computer integration procedures for calculating stress intensity factors around cracks subjected to complex stress fields, *Progress Report No.1: Stress and Fatigue-Fracture Design*, Petersburg Ontario, Canada, (1996).
- [25] Sadananda, K., Vasudevan, A.K., Kang, I.W., Effect of Superimposed Monotonic Fracture Modes on the  $\Delta K$  and  $K_{max}$  Parameters of Fatigue Crack Propagation, *Acta Materialia*, 51(22) (2003) 3399-3414.



- [26] Kajawski, D., A new  $(\Delta K + K_{max})^{0.5}$  driving force parameter for crack growth in aluminum alloys, *International Journal of Fatigue*, 23(8) (2001) 733-740.
- [27] Castillo, E., Galambos, J., Lifetime Regression Models Based on a Functional Equation of Physical Nature”, *Journal of Applied Probability*, 24 (1987) 160-169.
- [28] Castillo, E., Fernández-Canteli, A., Hadi, A.S., López-Anelle, M., A Fatigue Model with Local Sensitivity Analysis, *Fatigue and Fracture of Engineering Material and Structure*, 30 (2006) 149–168.
- [29] ASTM E606: Standard Practice for Strain-Controlled Fatigue Testing, *Annual Book of ASTM Standards*, ASTM, West Conshohocken, PA, USA, 03.01 (1998)
- [30] ASTM E647: Standard Test Method for Measurement of Fatigue Crack Growth Rates, *Annual Book of ASTM Standards*, ASTM, West Conshohocken, PA, USA, 03.01 (2000).
- [31] SAS, ANSYS, Swanson Analysis Systems, Inc., Houston, Version 12.0, (2011).
- [32] Ramberg, W., Osgood, W.R., Description of the stress-strain curves by the three parameters, NACA TN-902, National Advisory Committee for Aeronautics, (1943).